Gap solitons in rocking optical lattices and waveguides with undulating gratings

Thawatchai Mayteevarunyoo[1] and Boris A. Malomed[2]
[1]*Department of Telecommunication Engineering, Mahanakorn University of Technology, Bangkok 10530, Thailand*
[2]*Department of Physical Electronics, School of Electrical Engineering, Faculty of Engineering, Tel Aviv University, Tel Aviv 69978, Israel*

(Received 4 May 2009; published 27 July 2009)

We report results of a systematic analysis of the stability of one-dimensional solitons in a model including the self-repulsive or attractive cubic nonlinearity and a linear potential represented by a periodically shaking lattice, which was recently implemented in experiments with Bose-Einstein condensates. In optics, the same model applies to undulated waveguiding arrays, which are also available to the experiment. In the case of the repulsive nonlinearity, stability regions are presented, in relevant parameter planes, for fundamental gap solitons and their two-peak and three-peak bound complexes, in the first and second finite band gaps. In the model with the attractive nonlinearity, stability regions are produced for fundamental solitons and their bound states populating the semi-infinite gap. In the first finite and semi-infinite gaps, unstable solitons gradually decay into radiation, while, in the second finite band gap, they are transformed into more complex states, which may represent new species of solitons. For a large amplitude of the rocking-lattice drive, the model is tantamount to that with a "flashing" lattice potential, which is controlled by periodic sequences of instantaneous kicks. Using this correspondence, we explain generic features of the stability diagrams for the solitons. We also derive a limit case of the latter system, in the form of coupled-mode equations with a "flashing" linear coupling.

DOI: 10.1103/PhysRevA.80.013827 PACS number(s): 42.65.Tg, 03.75.Lm, 42.82.Et, 05.45.Yv

I. INTRODUCTION

Optical lattices (OLs) provide a highly efficient tool for the control of dynamics of collective excitations in Bose-Einstein condensates (BECs) [1]. In the experiment, OLs are created as interference patterns by coherent laser beams illuminating the condensate from opposite directions or by a set of parallel beams shone through an effectively one- or two-dimensional (1D or 2D) condensate. In photonics, the transmission of light beams may be controlled by counterparts of OLs in the form of gratings representing a periodic modulation of the refractive index in the direction transverse to the propagation axis of the probe beam. In particular, in photorefractive crystals, gratings may be induced by the interference of transverse beams with the ordinary polarization if the probe beam is launched in the extraordinary polarization [2]. In bulk silica, permanent material gratings can be written by means of a different optical technique [3]. The transverse structure of photonic-crystal fibers may also be considered, in a crude approximation, as a pattern of the periodic refractive-index modulation [4].

In experimental and theoretical studies of BEC, OLs were found to be especially efficient in supporting matter-wave solitons. It has been predicted that 2D and three-dimensional (3D) OLs can arrest the collapse and thus stabilize solitons, in the space of the same dimension, in the case of attractive interactions between atoms [5]. *Low-dimensional* 1D and 2D lattices, created, respectively, in the 2D [6] or 3D [6,7] space, may also stabilize multidimensional solitons, allowing them to move in the unrestricted direction [6]. Similarly, a cylindrical OL may lend the stability to 2D [8,9] and 3D [10] solitons. The stabilization of matter-wave solitons against the collapse was also analyzed in the framework of the 1D equation which combines the OL potential and nonpolynomial nonlinearity resulting from the tight confinement in the transverse plane [11].

In photonics, lattice structures have been used as a medium for the creation of spatial solitons which would not be possible otherwise. Notable results are (2+1)D fundamental [12], vortical [13], and necklace [14] solitons in photorefractive crystals equipped with the square-shaped lattice, as well as solitons supported by a photoinduced circular lattice [15]. Dipole-mode lattice solitons in a photorefractive medium featuring the self-defocusing nonlinearity were reported too [16]. The creation of solitons was also reported in bundled arrays of parallel waveguides inscribed in bulk silica [17]. Theoretically, various types of spatial solitons were investigated in models of 1D [18] and 2D [4] photonic crystals. The stability of localized vortices in photoinduced lattices [19], and of (2+1)D solitons in low-dimensional 1D lattices of the same type [20], was studied too.

For the case of repulsive interactions between atoms in BEC, it was predicted that stable gap solitons (GSs) could be supported by OL potentials, in both 1D [21] and multidimensional [22–26] geometries. Localized modes in the form of radial gap solitons were predicted in the 2D condensate trapped in an axisymmetric potential represented by a periodic function of the radial coordinate [9]. In the experiment, a GS was created in the condensate of ^{87}Rb atoms trapped in a quasi-1D configuration equipped with the longitudinal OL [1,27]. Then, extended confined states were discovered in the strong OL [28] and explained as segments of a nonlinear Bloch wave trapped in the OL potential [29].

Another theoretically studied versatile tool for steering the dynamics of nonlinear excitations in BEC is based on the periodic time modulation (*management* [30]) of various parameters affecting the condensate, such as the trap's strength in the cases of the self-repulsion [31] or attraction [32], and the periodic modulation of the nonlinearity strength, through the Feshbach resonance, by a low-frequency ac magnetic field (*Feshbach-resonance management*, FRM). It was predicted that FRM may stabilize 2D solitons [33], and also 3D ones, if combined with the one-dimensional OL potential [34]. In the 1D geometry proper, the FRM may support stable second-order soliton states [35] and multistability

[36]. Another species of robust localized modes, predicted to originate from the interplay between the OL in two or one dimensions and low-frequency FRM, represents *alternate solitons* adiabatically oscillating between GSs and ordinary solitons [37]. The action of the FRM on discrete solitons was studied too [38]. It is relevant to mention a related mechanism for the stabilization of 2D solitons against the collapse based on electromagnetically induced Rabi oscillations between two atomic states which feature opposite signs of the scattering length [39].

A natural extension of the study of the management techniques for BEC is to consider effects of periodic time modulation of the OL strength on the stability of solitons supported by the respective spatially periodic potential. The modulation can be easily realized by periodic attenuation of the intensity of the laser beams illuminating the condensate. For the attractive nonlinearity, a relevant problem is the identification of stability limits for 2D matter-wave solitons supported by the 1D [40] or full 2D [41] time-modulated OL potential (a similar problem for vortex solitons has not been considered yet). The same model applies to (2+1)D spatial solitons in bulk optical media, assuming that the transverse lattice structure is subjected to a periodic modulation along the propagation distance, similar to the setting proposed in Ref. [42]. The model with the transverse 1D lattice modulated in the longitudinal direction may also be realized in terms of spatiotemporal solitons running in a planar waveguide with an appropriate layered structure, similar to that considered in Ref. [43].

On the other hand, GSs in self-repulsive media do not exist at all without the lattice potential, therefore it is interesting to explore their stability limits under periodic variations of the lattice's amplitude. For the 1D setting, this analysis was performed in Ref. [44]. Note that the temporal modulation of the OL depth was used in the experiment aimed at transferring atom populations between different bands in the OL-induced spectrum embedded into a nearly 1D condensate [45]. Theoretical analysis, which predicts a ratchet transport and nonlinear resonances in the condensate loaded into the lattice, was performed too in models with the temporal modulation of the OL amounting to a periodic sequence of instantaneous flashes [46]. It remains to extend the theoretical investigation of the stability limits for GSs in the temporally modulated lattice to the multidimensional geometry.

Moving OLs are also available to the experiment [47]. The motion of the underlying interference pattern can be induced by the variation of the phase difference between the counterpropagating laser beams. Modulating the phase difference periodically in time, one can implement *rocking* (alias shaking) OLs, which move periodically back and forth. Recently, rocking OLs were used to demonstrate, in direct experiments, both a dynamical localization of matter-wave packets, through effective *suppression* of tunneling between local wells forming the OL potential, and (presumably) *enhancement* of the tunneling under specially selected conditions [48]. Dynamical localization of matter-wave packets due to the collapse of quasienergy bands [49] and transitions between the Mott insulator and superfluid in the rocking lattice were also studied experimentally [50].

In photonics, counterparts of rocking lattices are arrays of periodically curved waveguides. Remarkable effects have been demonstrated experimentally and described theoretically in undulated arrays that were permanently written, by means of the technique developed in Ref. [3], into bulk samples of silica [51]. These effects include all-optical beam steering [52], defect-free surface modes [53], inhibition of the light diffraction across the array [54], diffraction management [55], suppression of the coupling of guided discrete modes to the continuum [51], and various manifestations of the dynamical localization, self-collimation, and self-imaging of mono- and polychromatic wave packets [56]. In a different optical setting, using a photorefractive crystal, interband Rabi oscillations were experimentally demonstrated in a waveguiding array modulated along the propagation distance [57]. A model including a 2D rocking-lattice potential may also describe periodically twisted photonic-crystal fibers, such as those used in rocking optical filters [58].

In this work, we aim to identify stability limits for GSs and regular solitons in the framework of the 1D Gross-Pitaevskii or nonlinear Schrödinger equation (GPE/NLSE), which includes the repulsive or attractive cubic nonlinearity and the rocking-OL potential. This model directly applies to the above-mentioned physical settings for BEC and nonlinear optics alike. The model is introduced in Sec. II, where we also perform a simple analytical investigation, to demonstrate that, in the limit of a large rocking amplitude, the present model is tantamount to a variety of another recently studied one [46], with the above-mentioned *flashing* OL potential. We also derive its limit case in the form of coupled-mode equations with a *flashing* linear coupling, which corresponds to a narrow band gap (weak flashing potential).

The rest of the paper is organized as follows. Results for the GSs in the model with the repulsive nonlinearity are reported in Sec. III. They are summarized by means of diagrams showing stability borders for fundamental GSs and their bound complexes. Considered are families of GSs which reside, in the absence of the rocking, in the first two finite band gaps of the underlying linear spectrum. Some findings suggest that complex localized states different from the ordinary GSs may exist beyond the stability borders of the ordinary solitons, but systematic consideration of this issue is beyond the scope of the present work. In Sec. IV, stability diagrams are produced for regular solitons and their bound states populating the semi-infinite gap in the model with the attractive nonlinearity. Finally, in Sec. V, we give simple analytical estimates which explain certain features of the stability diagrams.

II. MODEL

A. Formulation

In the scaled form, the one-dimensional GPE/NLSE for the matter-wave wave function, ψ, or the amplitude of the guided electromagnetic wave, in the model combining the cubic nonlinearity (repulsive or attractive, for $\sigma=+1$ and -1, severally) and the rocking-lattice potential of amplitude V_0, is

$$i\frac{\partial\psi}{\partial t}=-\frac{1}{2}\frac{\partial^2\psi}{\partial x^2}+\sigma|\psi|^2\psi-V_0\cos\{2[x-\Xi\sin(\omega t)]\}\psi. \quad (1)$$

Here, t is the scaled time or propagation distance in the case of the atomic or photonic waves, respectively, x is the spatial coordinate (the transverse one, in the photonic model), which is scaled so as to make the lattice period equal to π, and (Ξ,ω) are the amplitude and frequency of the rocking modulation applied to the lattice. Being interested in solutions whose size is essentially smaller than the total length of the waveguide, we do not include a longitudinal trapping potential.

If Eq. (1) is derived from the underlying GPE for the 3D condensate [59], the scaled variables, t, x, and ψ, are related to their counterparts measured in physical units, T, X, and Ψ, as follows: $t \equiv T(\pi^2\hbar/md^2)$, $x \equiv \pi X/d$, and

$$\Psi(X,R,T) = \sqrt{\pi/(2|a_s|d^2)}\psi(x,t)\exp[-i\omega_\perp T - (\omega_\perp m/2\hbar)R^2], \tag{2}$$

where m is the atomic mass, d the OL period, and a_s the s-wave scattering length, while $\omega_\perp$ and R are the transverse trapping frequency and radial coordinate. If m is taken as the mass of ^{87}Rb atom and $d=1.5$ μm, then $\omega/2\pi=1$ corresponds, in physical units, to modulation frequency $\simeq 3$ kHz, while evolution time $t=10^4$, for which most results are presented below, translates into $\simeq 3$ s. Further, the scaled OL strength in Eq. (1) is $V_0=E_0/E_{\rm rec}$, where $E_{\rm rec}=(\pi\hbar)^2/(md^2)$ is the recoil energy and E_0 the depth of the periodic potential. In experiments with the ^{87}Rb condensate (which has $a_s=5.77$ nm), d varies between 0.4 and 1.6 μm, the corresponding scaled lattice depth being $V_0 \lesssim 20$. The negative sign in front of the potential term in Eq. (1) implies that the center of the soliton will be set at $x=0$, i.e., at a local potential minimum, in the absence of the rocking. In the application to optical waveguides, the relation of scaled NLSE (1) to the propagation equation written in physical units is well known too [56].

The single dynamical invariant of Eq. (1) is the norm, $N=\int_{-\infty}^{+\infty}|\psi(x,t)|^2dx$. According to Eq. (2), it is proportional to the total number of trapped atoms in the BEC, $N_{\rm atom}=(\pi a_\perp^2/a_s d)N$, where $a_\perp \equiv \sqrt{\hbar/(\omega_\perp m)}$ is the transverse-trapping radius. If, in particular, one takes $a_\perp \sim d \sim 1.5$ μm and $a_s \sim 1$ nm, then $N=1$ corresponds to $\simeq 5000$ atoms. In terms of the optical-beam transmission, N is proportional to the total power of the trapped light signal. Control parameters of the present model are V_0, ω, and Ξ, together with N.

B. Asymptotic form of the model with the large-amplitude rocking modulation

Using the Fourier decomposition, the rocking-OL potential in Eq. (1) can be transformed as follows:

$$\begin{aligned} U(x,t) &\equiv V_0\cos\{2[x-\Xi\sin(\omega t)]\} \\ &= V_0\{\cos[\Xi\sin(\omega t)]\cos(2x)+\sin[\Xi\sin(\omega t)]\sin(2x)\} \\ &= V_0\left\{\cos(2x)\left[J_0(\Xi)+2\sum_{p=1}^{\infty}J_{2p}(\Xi)\cos(2p\omega t)\right]\right. \\ &\quad \left.+2\sin(2x)\sum_{p=0}^{\infty}J_{1+2p}(\Xi)\sin[(1+2p)\omega t]\right\}, \end{aligned} \tag{3}$$

where J_n is the Bessel function. For large modulation amplitude Ξ, one can use the well-known approximation

$$J_n(\Xi) \approx \sqrt{\frac{2}{\pi\Xi}}\cos\left(\Xi-\frac{\pi}{4}(1+2n)\right) \tag{4}$$

to replace potential (3) by the following asymptotic form:

$$\begin{aligned} U(x,t) &\approx V_0\sqrt{\frac{2}{\pi\Xi}}\left\{\cos\left(\Xi-\frac{\pi}{4}\right)\cos(2x)\left[1+2\sum_{p=1}^{\infty}(-1)^p\cos(2p\omega t)\right]+2\left(\sin\Xi-\frac{\pi}{4}\right)\sin(2x)\sum_{p=0}^{\infty}(-1)^p\sin[(1+2p)\omega t]\right\} \\ &\equiv \frac{V_0}{\omega}\sqrt{\frac{2\pi}{\Xi}}\left\{2\cos\left(\Xi-\frac{\pi}{4}\right)\left[\sum_{n=-\infty}^{+\infty}\delta\left(t-\frac{\pi}{\omega}(2n+1)\right)\right]\cos(2x)\right. \\ &\quad \left.+\sin\left(\Xi-\frac{\pi}{4}\right)\sum_{n=-\infty}^{+\infty}\left[\delta\left(t-\frac{\pi}{\omega}\left(2n+\frac{1}{2}\right)\right)-\delta\left(t-\frac{\pi}{\omega}\left(2n-\frac{1}{2}\right)\right)\right]\sin(2x)\right\}, \end{aligned} \tag{5}$$

where $\delta(t)$ is the delta function. The validity of Eq. (5) can be checked via the Fourier decomposition of its right-hand side. Thus, in the limit of large Ξ, the rocking potential is effectively replaced by a superposition of two "flashing" OLs (cosinusoidal and sinusoidal ones), with the coefficients in front of $\cos(2x)$ and $\sin(2x)$ represented by periodic sequences of temporal kicks. The approximation based on Eq. (5) is used below to provide an explanation to some generic findings concerning the soliton stability.

C. Coupled-mode equations with the flashing coupling

In the case when the effective potential given by Eq. (5) is weak, i.e., the respective band gap is narrow, a natural approximation for the GS may be based on the linear combination of right- and left-traveling waves

$$\psi(x,t) = u(x,t)e^{ix-it/2}+v(x,t)e^{-ix-it/2}, \tag{6}$$

where $u(x,t)$ and $v(x,t)$ are slowly varying amplitudes. The substitution of ansatz (6) and potential (5) into Eq. (1) leads

to the coupled-mode equations (see, e.g., Ref. [25]). For instance, in the case of $\Xi=\pi/4+2\pi N$ with large integer N, these equations take the form of

$$i\frac{\partial u}{\partial t}+i\frac{\partial u}{\partial x}+\sigma(|u|^2+2|v|^2)u = \frac{V_0}{\omega}\sqrt{\frac{2\pi}{\Xi}}\left[\sum_{n=-\infty}^{+\infty}\delta\left(t-\frac{\pi}{\omega}(2n+1)\right)\right]v,$$

$$i\frac{\partial v}{\partial t}-i\frac{\partial v}{\partial x}+\sigma(|v|^2+2|u|^2)v = \frac{V_0}{\omega}\sqrt{\frac{2\pi}{\Xi}}\left[\sum_{n=-\infty}^{+\infty}\delta\left(t-\frac{\pi}{\omega}(2n+1)\right)\right]u. \quad (7)$$

Unlike the standard form of the coupled-mode equations, whose best known realization is presented by fiber Bragg gratings [60], Eqs. (7) feature the *flashing coupling* between the two modes (rather than the constant coupling). In this work, we do not investigate the model based on Eqs. (7), but it may be interesting to study the existence and stability limits for GSs in it.

III. GAP SOLITONS IN THE MODEL WITH THE SELF-DEFOCUSING NONLINEARITY

A. Gap solitons in the static optical lattice

First we consider the case of the self-repulsive nonlinearity, i.e., $\sigma=+1$ in Eq. (1), when the OL supports localized modes in the form of GSs. Before proceeding to the presentation of findings for the rocking OL, it is relevant to briefly recapitulate known results for one-dimensional GSs in the static OL, with $\Xi=0$. We here consider solutions that, in the limit of $\Xi=0$, populate two lowest finite band gaps of the spectrum generated by the linearized version of Eq. (1). The respective stationary solutions with chemical potential μ (alias propagation constant $-\mu$, in terms of optics) are looked for as $\psi(x,t)=\exp(-i\mu t)\phi(x)$, with real function ϕ obeying an ordinary differential equation

$$\mu\phi+\frac{1}{2}\frac{d^2\phi}{dx^2}+V_0\cos(2x)\phi+\sigma\phi^3=0. \quad (8)$$

Once solutions to Eq. (8) have been found, their stability can be examined by looking for a perturbed solution to Eq. (1) with $\Xi=0$ as $\psi(t,x)=\exp(-i\mu t)[\phi(x)+ue^{i\lambda t}+v^*e^{i\lambda^* t}]$, where $u(x)$ and $v(x)$ are eigenmodes of the infinitesimal perturbation pertaining to eigenvalue λ (generally, it may be a complex one). The subsequent linearization of Eq. (1) gives rise to a linear problem

$$\begin{pmatrix}\hat{L} & \sigma\phi^2\\ -\sigma\phi^2 & -\hat{L}\end{pmatrix}\begin{pmatrix}u\\ v\end{pmatrix}=\lambda\begin{pmatrix}u\\ v\end{pmatrix}, \quad (9)$$

with $\hat{L}\equiv-(1/2)d^2/dx^2-\mu+V_0\cos(2x)+2\sigma\phi^2(x)$. The underlying solution, ϕ, is stable if all eigenvalues λ are real.

As shown in a number of works [21–24,44,61], Eq. (8) gives rise to families of single-peak solutions (fundamental GSs) and in-phase or out-of-phase multipeak complexes (bound states of the fundamental solitons). In addition to these, in the second band gap, one can also find *subfundamental solitons* (SFSs), which feature a pair of antisymmetric peaks squeezed into a single cell of the periodic potential [24,44,61]. Following Ref. [44], we call them subfundamental modes because their norm is lower than that of the fundamental GSs existing in the second band gap at the same values of chemical potential μ. The SFSs are unstable in nearly the entire second band gap [44], except for a narrow interval of values of μ adjacent to the left edge of the band gap, where the SFS are stable, while the fundamental GSs do not exist there (see Fig. 1 below) [61]. Being unstable almost everywhere at $\Xi=0$, the SFS do not have a chance to give rise to generic families of stable modes in the rocking OL, therefore we do not consider them below.

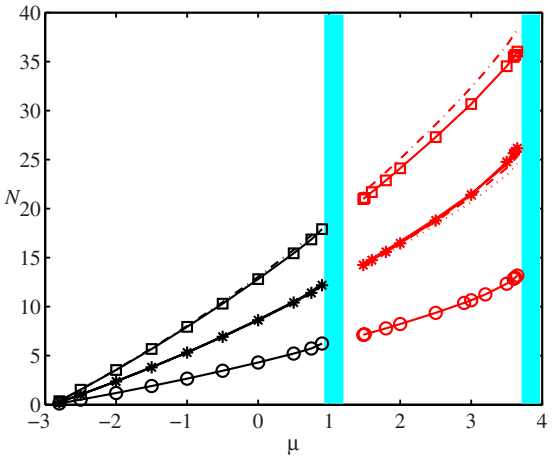

FIG. 1. (Color online) Basic families of gap solitons in the model combining the self-repulsive nonlinearity and the static OL ($\Xi=0$, $V_0=5$) are shown here by means of respective $N(\mu)$ curves in the first and second finite band gaps. Circles: fundamental gap solitons [examples are shown in Fig. 2(a)]. Solid curve without symbols and the chain of stars represent, respectively, in-phase (symmetric) two-peak "densely packed" bound states, without an empty cell between the peaks, and their counterparts with the empty cell [see examples in Figs. 2(b) and 2(c)]. Dotted and dashed curves: out-of-phase (antisymmetric) two-peak bound states, without or with an empty cell between the two peaks, respectively [see Figs. 2(d) and 2(e)]. Dashed-dotted curve: in-phase three-peak bound states, see examples in Fig. 2(f); squares: out-of-phase three-peak complexes [see Fig. 2(g)]. In the first band gap, the $N(\mu)$ curves for all two-peak states are almost undistinguishable, as well as the curves for the different three-peak states.

Families of fundamental GSs and their two- and three-peak bound states (both in-phase and out-of-phase ones) are represented by respective $N(\mu)$ curves in Fig. 1, for OL strength $V_0=5$, which is fixed as it adequately represents the generic case. In accordance with what was said above, fundamental GSs do not exist in a narrow interval of values of μ close to the left edge of the second finite band gap. As concerns in-phase and out-of-phase two-peak bound states, the diagram includes their families of different types, *viz.*, "densely packed" ones, with no empty lattice site between the two peaks and a variety featuring an empty cell between the peaks.

Generic examples of stable and unstable single- and multipeaked GSs in both the first and second finite band gaps are displayed in Fig. 2, along with sets of eigenvalues which determine their stability in the linear approximation. In the first band gap, all the GS families presented in Fig. 1 are stable. In fact, most important for the possibility of the experimental creation of solitons is not their stability against infinitely small perturbations, which is illustrated by eigenvalues shown in Fig. 2, but the robustness against finite disturbances, which should be tested in direct simulations. To test the localized modes in this respect, we ran simulations of their evolution, replacing, in the initial conditions, stationary profiles $u(x)$ by perturbed ones

$$\psi_{\text{pert}}(x) = u(x)[1 + \varepsilon\rho(x)], \tag{10}$$

where $\rho(x)$ is a random functions with an amplitude ~ 1 (it was actually generated by means of the standard MATLAB's feature, "rand") and ε is a small amplitude of the perturbation. The simulations were performed by means of the split-step Fourier-transform method, with absorbers placed at edges of the integration domain. The domain was covered by a mesh consisting of $N=512$ grid points and the step size of the time integration was $\Delta t=0.005$. Results of such simulations, shown in Fig. 3, demonstrate that most sensitive to the addition of finite perturbations are the out-of-phase bound states of the types shown in Figs. 2(d) and 2(g)—in the sense that these states tend to trap the perturbation rather than readily relaxing back into the unperturbed state. This feature may be explained by the fact that the respective two- and three-peak complexes include deep notches between repelling density maxima, which may trap the perturbation. The symmetric bound state with an empty cell between the peaks is also somewhat more sensitive to the perturbation that its "densely packed" counterpart [cf. Figs. 3(c) and 3(b)]. Nevertheless, Fig. 3 clearly suggests that these GS complexes are stable in the first finite band gap.

In the second band gap, the fundamental solitons are also stable, in the direct simulations, in the region where they exist, *viz.*, for $1.48 < \mu < 3.725$ (see Fig. 1). However, an essential caveat is that, close to the right edge of the band gap, the fundamental solitons become loosely bound, developing conspicuous weakly localized "tails," as shown in Fig. 4(a) for $\mu=3.7$. If the evolution of such a perturbed soliton is simulated, it remains stable [see Fig. 4(b)], provided that the size of integration domain is sufficiently large. On the other hand, if the integration domain is not wide enough, "chopping off" parts of the soliton's tails, the addition of the (weak) perturbation may destabilize the soliton, initiating its rearrangement into a "lighter" counterpart, through shedding off a considerable part of its norm [see an example in Fig. 4(c)]. The final stable soliton stays in the second band gap [in the case displayed in Fig. 4(c), it has $\mu \approx 2.00$ and norm $N=8.23$, which implies the loss of about 40% of the initial norm]. In the real physical situation, both cases are possible, as the experimental domain (for instance, the transverse size of the optical sample in which the waveguiding array was inscribed [3]) may be either broad or relatively narrow.

All multipeak complexes are unstable in the second band gap. Among them, in-phase and out-of-phase (symmetric and antisymmetric) two-peak modes with an empty cell in the middle appear as nearly stable solutions, as the computation of the respective stability eigenvalues yields a quartet with very small imaginary parts [roughly, 50 times smaller than their counterparts responsible for the instability of the two-peak antisymmetric state at the same μ, but without the empty cell, cf. Figs. 2(c), 2(e), 2(b), and 2(d)]. The weakness of the instability in this case is explained by the fact that the interaction between the far-separated peaks in the respective bound states is weaker than in other complexes.

B. Stability of gap solitons in the rocking optical lattice

The stability of various species of GSs supported by the OL subjected to the rocking modulation, with $\Xi \neq 0$ in Eq. (1), was analyzed by means of systematic simulations of the evolution of these solitons using the split-step algorithm. Of course, it makes sense to explore the effective stability under the rocking modulation of those GS species that were stable at $\Xi=0$. The solitons were identified as stable against the rocking if, in the course of very long simulations, they would feature shuttle motion without tangible loss of the norm; technically, the solitons were identified as definitely stable ones if they lost less than 0.1% of the initial norm in the course of the simulations lasting up to $t=10\,000$ (in the case of the low-frequency modulation, the simulations were extended to $t=100\,000$ to make their stability certain, see Fig. 5 below). On the contrary, unstable solitons which originate in the first finite band gap clearly demonstrate gradual decay into radiation (without a trend to rearrange themselves into any other stable mode; the situation is different in the second band gap, as explained below).

To illustrate the definition of the effective stability of the GSs driven by the rocking OL, typical examples of stable and unstable two-soliton antisymmetric bound states, with the empty cell at the center, which belong (at $\Xi=0$) to the first finite band gap, are displayed in Figs. 5 and 6. Actually, these examples also illustrate the definition of the stability and instability for fundamental GSs, as the corresponding bound fundamental solitons are not conspicuously altered by the interaction. As concerns the case shown in Fig. 5, it is relevant to note that the total simulation time, $t=100\,000$, is equivalent to ≈ 8000 periods of the low-frequency rocking, which is definitely sufficient to make conclusions about the stability of the OL-driven soliton.

Note that the sampling frequency used in Fig. 5(a), which is $\omega_{\text{sampl}}=2\pi/1000$ (see the caption to the figure), features a small mismatch with the rocking frequency, $\Delta\omega \equiv 8\omega_{\text{sampl}} - \omega \approx 2.65 \times 10^{-4}$, the respective beating period being $2\pi/\Delta\omega \approx 23\,700$. This estimate explains the fact that Fig. 5(a) displays, effectively, slightly more than four full cycles of the oscillations in the time interval of $0 < t < 100\,000$.

In the second finite band gap, the instability exhibited by the fundamental GSs under the action of the rocking is completely different from what was observed in the first band gap. Namely, while the GS, which is identified as a stable one, performs the shuttle motion in the intact state [see a typical example in Fig. 7(a)], its unstable counterpart quickly splits into several components, rather

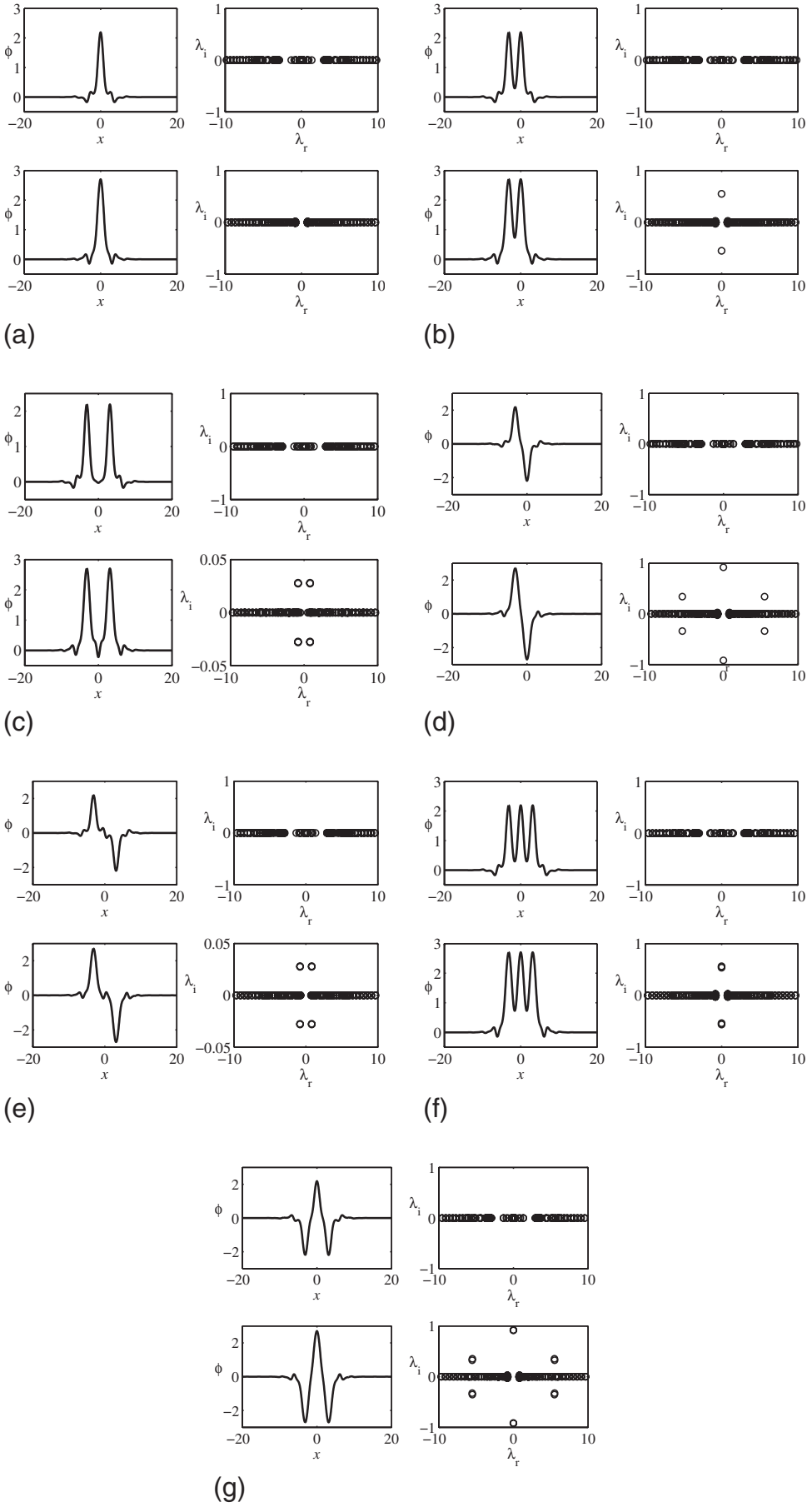

FIG. 2. Examples of soliton profiles, and complex planes of the respective stability eigenvalues, in the first and second finite band gaps (upper and lower plots in each panel, respectively) at $\mu=0.8$ and $\mu=3.0$.

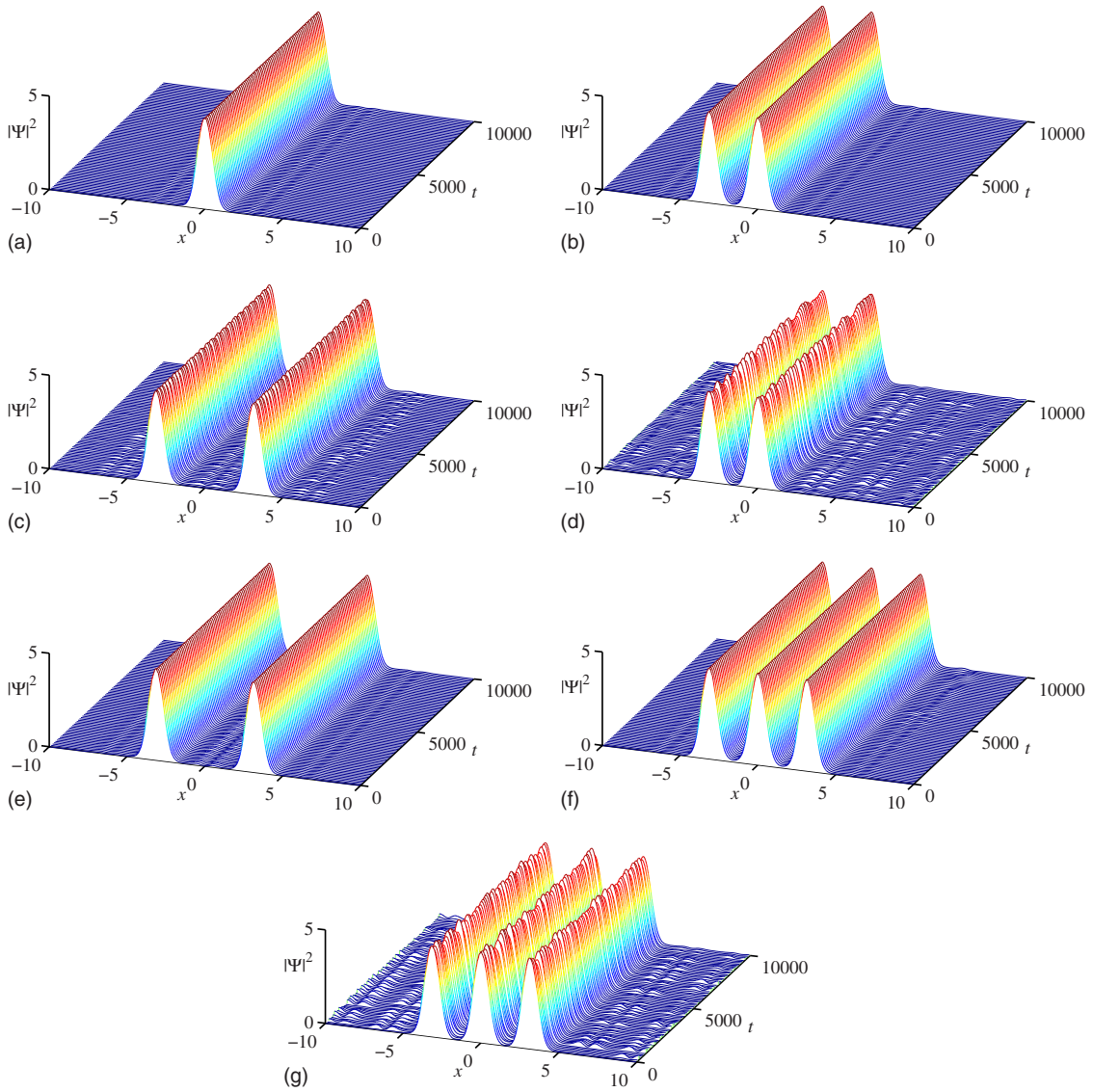

FIG. 3. (Color online) The evolution of gap solitons from the first band gap, shown in Fig. 2, under the action of random initial perturbation (10) with amplitude $\varepsilon=0.01$.

than featuring a slow decay, as shown in Fig. 7(b). The complex state resulting from the splitting is, by itself, quite robust, although it cannot be identified as a fundamental soliton. It is plausible that the localized mode displayed in Fig. 7(b) is an example of another type of (quasi-)solitons that may be supported by the rocking lattice beyond the border of the instability of ordinary GSs. However, detailed investigation of this issue is beyond the scope of the present work.

We note that, with the sampling frequencies $\omega_{\text{sampl}}=2\pi/100$ in Figs. 7(a) and 7(b) (as per the caption to Fig. 7), the corresponding frequency mismatch is the same in both cases, $\Delta\omega\equiv 8\omega_{\text{sampl}}-\omega\approx 0.002\,65$, which yields the beating period, $2\pi/\Delta\omega\approx 2370$. The latter number explains the fact that one can see a bit more than four full oscillations of the solitons in both panels of Fig. 7.

Results of the systematic simulations are summarized in Figs. 8 and 9, which show stability regions for fundamental GSs and two- and three-peak bound complexes in the parameter planes of (N,Ξ), for fixed ω, and in the plane of (Ξ,ω), for fixed N. Figure 8 includes the results for the fundamental solitons in both the first and second finite band gaps, while Fig. 9 appertains only to the first band gap. All multipeak states whose stability areas are displayed in Fig. 8 belong solely to the first gap too. Note that the stability area for the fundamental GSs is much larger in the first finite band gap than in the second band gap. The figures do not include the family of "densely packed" antisymmetric bound states, without the empty cell in the middle (from the first finite band gap), as this family is completely destabilized by the rocking, even at very small values of Ξ. In keeping with the same trend, the stability areas for the densely packed symmetric bound states in Figs. 8 and 9 are much smaller than for their counterparts featuring the empty site between the peaks.

It is worthy to note that the shape of the stability regions in Fig. 8 is generally similar to that reported in Ref. [44] for fundamental GSs and their bound states

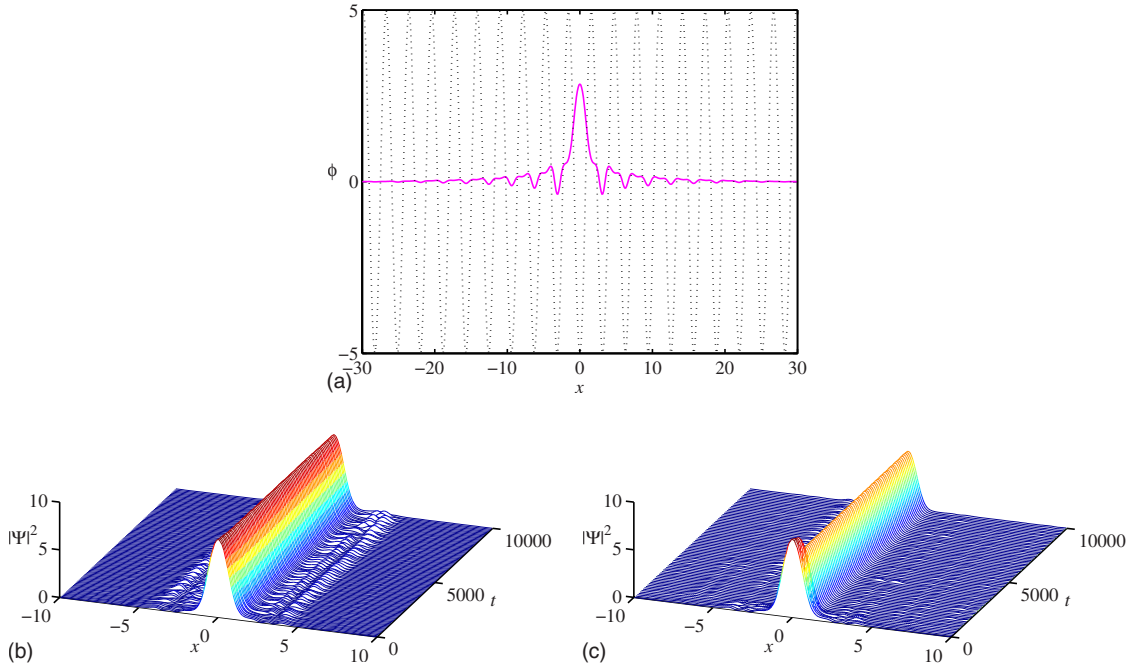

FIG. 4. (Color online) (a) The "loosely bound" profile of a fundamental soliton found at $\mu=3.7$, i.e., very close to the right edge of the second band gap [cf. its "tightly bound "counterpart corresponding to $\mu=3.0$, i.e., located in the middle of the second band gap, which is shown in bottom plot of Fig. 2(a)]. In this panel, the dotted line depicts the underlying periodic potential. (b) The evolution of the perturbed soliton from panel (a) in a broad integration window of width $L=60$, under the action of perturbation (10), with $\varepsilon=0.01$ (for stronger perturbations, the results are quite similar). (c) The same as in (b), in the integration window twice as narrow, with $L=30$.

in the 1D model with the time-periodic modulation applied to the amplitude of the OL. An explanation to some generic features of the stability diagrams is given below in Sec. V.

IV. SELF-FOCUSING MODEL

A. Solitons in the static lattice

In the model with the self-attractive nonlinearity, i.e., $\sigma=-1$ in Eq. (1) and static OL potential ($\Xi=0$), usual solitons of various types can be readily found in the semi-infinite gap, following Ref. [62]. For the sake of comparison to the rocking-OL model, a set of curves $N(\mu)$ for different families of stable solitons in the static model is displayed in Fig. 10 and typical examples of such solitons are shown in Fig. 11.

B. Stability of solitons in the rocking lattice

Systematic simulations of Eq. (1) with $\sigma=-1$ demonstrate that the fundamental solitons which populate the semi-

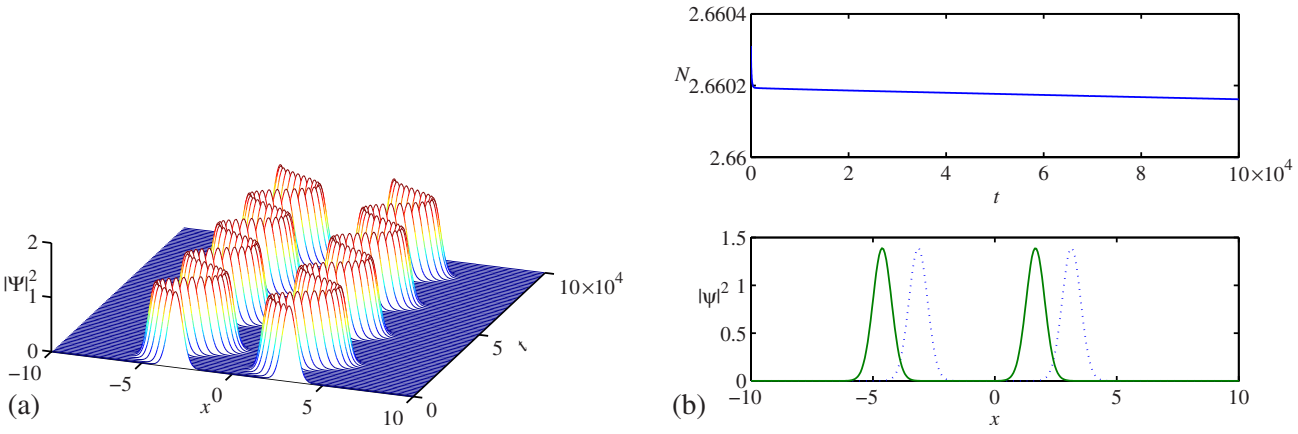

FIG. 5. (Color online) An antisymmetric (out-of-phase) bound state of two fundamental gap solitons belonging to the first band gap, with an empty cell in the middle, which remains stable under the action of the rocking with $\omega=0.05$ and $\Xi=1.5$. Before the application of the rocking, parameters of the bound state were $N=2.66$ and $\mu=-1.90$. (a) The motion of the soliton trapped by the rocking lattice. The field profiles are displayed through intervals $\Delta t_{\text{sampl}}=1000$. Top and bottom parts of panel (b) display, respectively, the dependence of the norm on time and the comparison of initial and final shapes of the bound state.

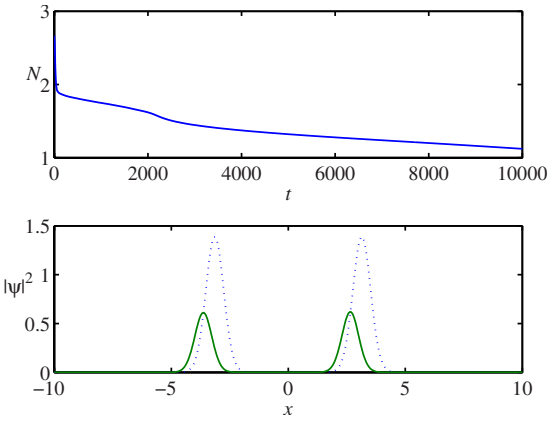

FIG. 6. (Color online) The same as in Fig. 5(b), but for rocking-modulation frequency $\omega=1$. In this case, the antisymmetric bound state is clearly unstable due to systematic loss of the norm.

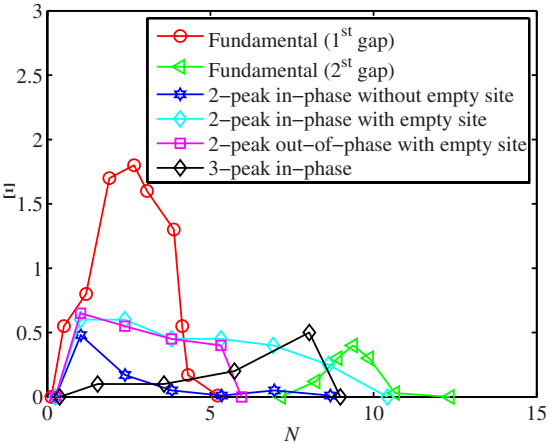

FIG. 8. (Color online) Stability borders for fundamental gap solitons and their bound complexes in the plane of the soliton's norm (N) and rocking amplitude (Ξ). The strengths of the optical lattice and modulation frequency are fixed: $V_0=5$ and $\omega=0.5$. In the absence of the modulation, all bound states belong to the first finite band gap. "Two-peak in-phase" are symmetric bound states, with or without the empty cell between the peaks, as in Figs. 2(b) and 2(c), respectively. "Two-peak out-of-phase" complexes are antisymmetric ones, with the empty cell in the middle [see Fig. 2(e)] while their densely packed counterparts, without the empty cell [see Fig. 2(d)], are completely unstable under the action of the rocking.

infinite gap at $\Xi=0$, as well as symmetric and antisymmetric two-peak bound states may remain stable in the rocking lattice. As concerns three-peak complexes, their in-phase variety survives in a considerable parameter region, while three-peak bound states of the out-of-phase type are very quickly destroyed by the rocking. The distinction between stable and unstable solitons in the semi-infinite gap is similar to that in the first finite band gap, in the case of the self-repulsive nonlinearity (see above): stable states perform the shuttle motion under the action of the rocking drive without any manifestation of the decay, while their unstable counterparts demonstrate a persistent decay, losing nearly all the initial norm by $t\sim 500$. No trend to rearrangement of unstable solitons into new robust modes has been found in this situation.

To summarize the findings made in the framework of the self-focusing model, in Fig. 12 we display stability borders for the solitons in the plane of (N,Ξ), with fixed $V_0=5$ and $\omega=0.5$ (cf. Fig. 8). Stability borders in the plane of (Ξ,ω) (cf. Fig. 9) are drawn in Fig. 13 for fixed $N=3.5$ and $V_0=5$. Comparison of these figures with Figs. 8 and 9 demonstrates that the shapes of the borders of the stability regions for the solitons in the self-focusing model are, roughly, similar to those for the GSs in the self-defocusing model. Nevertheless, a noteworthy difference is that, while in the model with the self-repulsive nonlinearity, the fundamental GSs clearly feature the largest stability area (in any parameter plane), the largest stability regions in the self-attraction model appertain to two-peak complexes, rather than fundamental solitons.

V. ANALYTICAL ESTIMATES

Some generic features of the numerical findings can be explained using approximation (5) and Eq. (3). In the case of the self-defocusing model, the variational approximation predicts [37] that the stationary OL potential, taken as $\epsilon\cos(2x)$, may support tightly bound (strongly localized) GSs in the first band gap provided that the OL strength exceeds a threshold value

$$|\epsilon| > \epsilon_0 \equiv e^2/16. \tag{11}$$

On the other hand, the time average of the rocking potential in Eq. (3) is

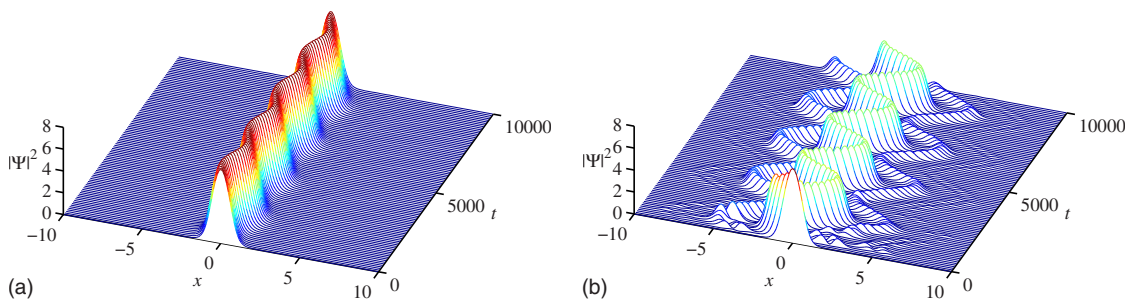

FIG. 7. (Color online) Typical examples of fundamental gap solitons from the second finite band gap (with $\mu=2.5$) that, respectively, (a) remain stable or (b) become unstable if subjected to the action of the rocking with $\omega=0.5$ and (a) $\Xi=0.3$ or (b) $\Xi=1.5$. The sampling interval in both panels is $\Delta t_{\text{sampl}}=100$.

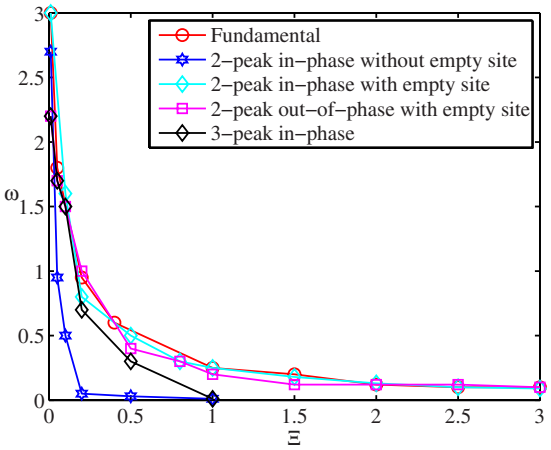

FIG. 9. (Color online) Stability borders for fundamental gap solitons and bound complexes in the plane of the rocking-modulation parameters, (Ξ,ω), in the first finite band gap. The norm and lattice strength are fixed here: $N=3.46$ and $V_0=5$.

$$\langle U(x)\rangle = V_0 J_0(\Xi)\cos(2x). \tag{12}$$

In this expression, the effective OL's amplitude is identified as $\epsilon=V_0J_0(\Xi)$, hence threshold condition (11) takes the form of $J_0(\Xi)>e^2/(16V_0)\approx 0.092$—for $V_0=5$, which was used in the numerical simulations. With the lowest root of equation $J_0(\Xi)=0.092$ being $\Xi_{\rm cr}\simeq 2.25$, the present consideration predicts that GSs originating from the first band gap cannot be supported by the rapidly rocking OL at $\Xi>\Xi_{\rm cr}$. This rough estimate may explain the most salient feature observed in Fig. 8, *viz.*, the nonexistence of stable GSs at $\Xi>\Xi_{\rm cr}\simeq 1.8$ (the moderate discrepancy in the value of $\Xi_{\rm cr}$ may be accounted for by the fact that Fig. 6 pertains to $\omega=0.5$, which does not exactly imply rapid rocking).

This explanation does not apply to the self-focusing version of the model, which admits the existence of solitons in the semi-infinite gap for any strength ϵ of the periodic potential. In fact, the destabilization of NLSE solitons under the action of time-periodic "management" has a more complex character and it cannot be analyzed by means of such a rough approximation [30,63].

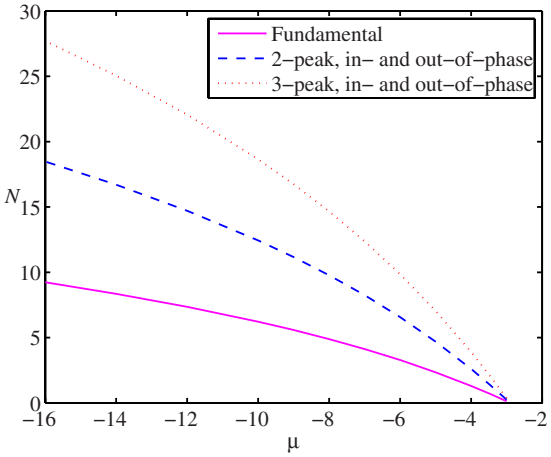

FIG. 10. (Color online) Lowest-order families of solitons in the self-focusing model with the static lattice (of strength $V_0=5$) are shown by means of $N(\mu)$ dependences. These curves are virtually identical for the bound-state families of the in-phase and out-of-phase types.

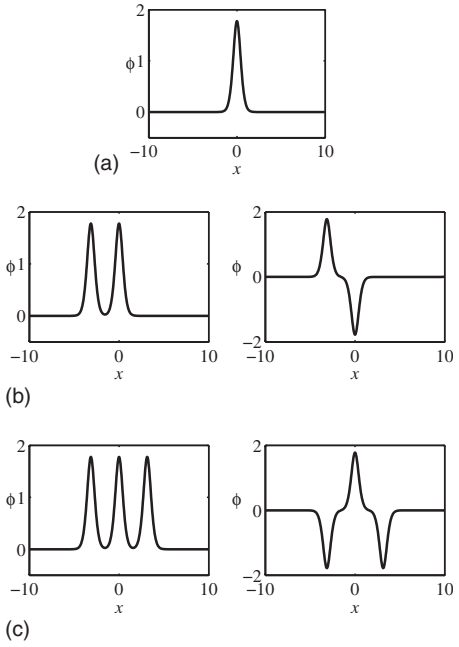

FIG. 11. Profiles of stable solitons in the self-focusing model with the static lattice ($\Xi=0$, $V_0=5$) and $\mu=5$. (a) A fundamental soliton; (b) a densely packed two-soliton bound state; (c) a three-soliton bound state.

Nevertheless, the form of the stability border in Fig. 11 at large Ξ can be explained using approximation (5). Indeed, in the case of large Ξ and small ω, Eq. (5) reduces the rocking potential to the superposition of three periodic sequences of kicks, with large period $2\pi/\omega$. Because each kick multiplies the wave function by potential $\cos(2x)$ or $\sin(2x)$, it instantaneously imprints the respective phase profile, $\varphi(x)$, onto the soliton, lending it the corresponding *phase chirp*, $\varphi''(x)$. Thus, the stability of the soliton under the action of the low-

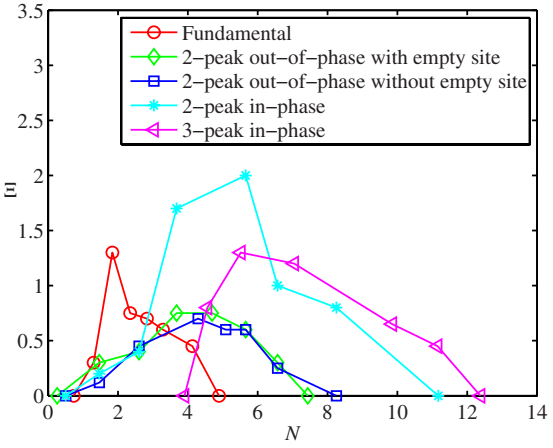

FIG. 12. (Color online) Stability borders for fundamental solitons and their bound states in the plane of (N,Ξ) of the model with the self-focusing nonlinearity and fixed parameters $V_0=5$ and $\omega=0.5$.

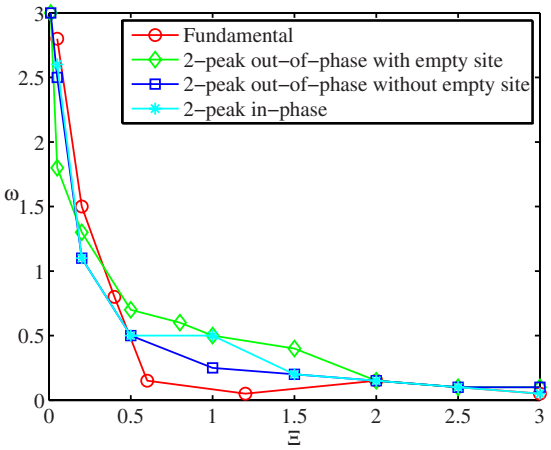

FIG. 13. (Color online) Stability borders for fundamental solitons and two-peak bound states in the model with the self-focusing nonlinearity, in the plane of (Ξ,ω). The norm is fixed to $N=3.5$.

frequency large-amplitude rocking modulation, in the self-focusing model, amounts to the survival of the NLSE soliton after the chirp was instantaneously imprinted onto it. The latter problem can be solved by means of the variational approximation [64] or, in an exact form, using the inverse scattering transform for the integrable NLSE (ignoring, for that purpose, the presence of the lattice) [65]. The result is that the soliton survives if the value of the chirp imprinted at its center does not exceed a certain critical value. On the other hand, the strength of the kicks in Eq. (5) is $\sqrt{2\pi}V_0/(\sqrt{\Xi}\omega)$, hence the stability border should take the form of $\omega=\text{const}/\sqrt{\Xi}$, which qualitatively complies with the shape observed in Fig. 13.

VI. CONCLUSION

In this work, we have developed the stability analysis for 1D solitons in the model including the self-defocusing or focusing nonlinearity, in combination with the potential of the rocking lattice. The model has straightforward implementations in the form of periodically shaking OLs, which have recently attracted attention in experiments with BEC, and in nonlinear optics, in terms of periodically curved waveguiding arrays, which were recently made available to the experiment.

The work was focused on the identification of rocking-induced stability limits for solitons which are stable in the absence of the rocking. In the case of the self-repulsive nonlinearity, the analysis was performed for GSs in the two lowest finite band gaps. In the model with the attractive nonlinearity, the stability of regular solitons populating the semi-infinite gap was studied. The results were summarized in the form of stability diagrams, in relevant parameter planes, for fundamental solitons and two- and three-peak bound complexes of different parities (in-phase and out-of-phase types). Two distinct types of symmetric and antisymmetric two-peak states were considered: "densely" and "loosely" packed ones, i.e., without an empty cell between the peaks or with the empty cell included. In the semi-infinite gap, as well as in the first finite band gap, stable and unstable solitons are distinguished, respectively, as persistent localized states, which perform the shuttle motion under the action of the rocking lattice, or gradually decaying localized modes. In the second finite band gap, fundamental GSs which were identified as unstable under the action of the rocking do not decay into radiation, but rather feature splitting into new complex states. Plausibly, the latter ones may represent novel (quasi-)localized modes that may exist beyond the stability borders of the ordinary GSs. In the limit of the large rocking amplitude, the model is tantamount to a special case of the system with a flashing lattice, driven by three periodic sequences of instantaneous kicks. Using this representation of the rocking lattice, some generic features of the stability diagrams for solitons were explained.

This work can be extended in other directions, one natural possibility being the consideration of the rocking lattice in two dimensions, for both signs of the nonlinearity. Another challenging issue is the search for persistently moving solitons driven by the rocking lattice. Our preliminary analysis of this issue demonstrates that the application of an initial kick to the soliton easily results in its eventual destruction in the present setting. As mentioned above, it may also be interesting to identify effective stability limits for solitons in the framework of the coupled-mode equations with the "flashing" linear coupled, i.e., Eqs. (7).

ACKNOWLEDGMENT

We appreciate valuable discussions with O. Morsch.

[1] O. Morsch and M. Oberthaler, Rev. Mod. Phys. **78**, 179 (2006).

[2] N. K. Efremidis, S. Sears, D. N. Christodoulides, J. W. Fleischer, and M. Segev, Phys. Rev. E **66**, 046602 (2002); N. K. Efremidis, J. Hudock, D. N. Christodoulides, J. W. Fleischer, O. Cohen, and M. Segev, Phys. Rev. Lett. **91**, 213906 (2003); J. W. Fleischer, G. Bartal, O. Cohen, T. Schwartz, O. Manela, B. Freedman, M. Segev, H. Buljan, and N. K. Efremidis, Opt. Express **13**, 1780 (2005).

[3] T. Pertsch, U. Peschel, F. Lederer, J. Burghoff, M. Will, S. Nolte, and A. Tünnermann, Opt. Lett. **29**, 468 (2004); A. Szameit, D. Blömer, J. Burghoff, T. Schreiber, T. Pertsch, S. Nolte, A. Tünnermann, and F. Lederer, Opt. Express **13**, 10552 (2005).

[4] P. Xie, Z.-Q. Zhang, and X. Zhang, Phys. Rev. E **67**, 026607 (2003); A. Ferrando, M. Zacarés, P. F. de Cordoba, D. Binosi, and J. A. Monsoriu, Opt. Express **11**, 452 (2003).

[5] B. B. Baizakov, B. A. Malomed, and M. Salerno, Europhys. Lett. **63**, 642 (2003); J. Yang and Z. H. Musslimani, Opt. Lett. **28**, 2094 (2003); Z. H. Musslimani and J. Yang, J. Opt. Soc.

Am. B **21**, 973 (2004); J. Yang, I. Makasyuk, A. Bezryadina, and Z. Chen, Stud. Appl. Math. **113**, 389 (2004); Z. Shi and J. Yang, Phys. Rev. E **75**, 056602 (2007); A. Gubeskys and B. A. Malomed, Phys. Rev. A **76**, 043623 (2007); T. Mayteevarunyoo, B. A. Malomed, B. B. Baizakov, and M. Salerno, Physica D **238**, 1439 (2009).

[6] B. B. Baizakov, B. A. Malomed, and M. Salerno, Phys. Rev. A **70**, 053613 (2004); L. Gubeskys and B. A. Malomed, *ibid.* **79**, 045801 (2009).

[7] D. Mihalache, D. Mazilu, F. Lederer, Y. V. Kartashov, L.-C. Crasovan, and L. Torner, Phys. Rev. E **70**, 055603(R) (2004).

[8] Y. V. Kartashov, V. A. Vysloukh, and L. Torner, Phys. Rev. Lett. **93**, 093904 (2004); **94**, 043902 (2005); Y. V. Kartashov, R. Carretero-González, B. A. Malomed, V. A. Vysloukh, and L. Torner, Opt. Express **13**, 10703 (2005).

[9] B. B. Baizakov, B. A. Malomed, and M. Salerno, Phys. Rev. E **74**, 066615 (2006).

[10] D. Mihalache, D. Mazilu, F. Lederer, B. A. Malomed, Y. V. Kartashov, L.-C. Crasovan, and L. Torner, Phys. Rev. Lett. **95**, 023902 (2005).

[11] L. Salasnich, A. Cetoli, B. A. Malomed, and F. Toigo, Phys. Rev. A **75**, 033622 (2007).

[12] J. W. Fleischer, M. Segev, N. K. Efremidis, and D. N. Christodoulides, Nature (London) **422**, 147 (2003).

[13] D. N. Neshev, T. J. Alexander, E. A. Ostrovskaya, Y. S. Kivshar, H. Martin, I. Makasyuk, and Z. Chen, Phys. Rev. Lett. **92**, 123903 (2004); J. W. Fleischer, G. Bartal, O. Cohen, O. Manela, M. Segev, J. Hudock, and D. N. Christodoulides, *ibid.* **92**, 123904 (2004).

[14] J. Yang, I. Makasyuk, P. G. Kevrekidis, H. Martin, B. A. Malomed, D. J. Frantzeskakis, and Z. Chen, Phys. Rev. Lett. **94**, 113902 (2005).

[15] X. Wang, Z. Chen, and P. G. Kevrekidis, Phys. Rev. Lett. **96**, 083904 (2006).

[16] L. Tang, C. Lou, X. Wang, D. Song, X. Chen, J. Xu, Z. Chen, H. Susanto, K. Law, and P. G. Kevrekidis, Opt. Lett. **32**, 3011 (2007).

[17] A. Szameit, J. Burghoff, T. Pertsch, S. Nolte, A. Tünnermann, and F. Lederer, Opt. Express **14**, 6055 (2006); A. Szameit, T. Pertsch, F. Dreisow, S. Nolte, A. Tünnermann, U. Peschel, and F. Lederer, Phys. Rev. A **75**, 053814 (2007).

[18] T. Mayteevarunyoo and B. A. Malomed, J. Opt. Soc. Am. B **25**, 1854 (2008).

[19] J. Yang, New J. Phys. **6**, 47 (2004).

[20] T. Mayteevarunyoo and B. A. Malomed, Phys. Rev. E **73**, 036615 (2006).

[21] F. Kh. Abdullaev, B. B. Baizakov, S. A. Darmanyan, V. V. Konotop, and M. Salerno, Phys. Rev. A **64**, 043606 (2001); I. Carusotto, D. Embriaco, and G. C. La Rocca, *ibid.* **65**, 053611 (2002).

[22] B. B. Baizakov, V. V. Konotop, and M. Salerno, J. Phys. B **35**, 5105 (2002).

[23] P. J. Y. Louis, E. A. Ostrovskaya, C. M. Savage, and Y. S. Kivshar, Phys. Rev. A **67**, 013602 (2003).

[24] N. K. Efremidis and D. N. Christodoulides, Phys. Rev. A **67**, 063608 (2003).

[25] H. Sakaguchi and B. A. Malomed, J. Phys. B **37**, 2225 (2004).

[26] Z. Shi, J. Wang, Z. Chen, and J. Yang, Phys. Rev. A **78**, 063812 (2008).

[27] B. Eiermann, Th. Anker, M. Albiez, M. Taglieber, P. Treutlein, K.-P. Marzlin, and M. K. Oberthaler, Phys. Rev. Lett. **92**, 230401 (2004).

[28] Th. Anker, M. Albiez, R. Gati, S. Hunsmann, B. Eiermann, A. Trombettoni, and M. K. Oberthaler, Phys. Rev. Lett. **94**, 020403 (2005).

[29] T. J. Alexander, E. A. Ostrovskaya, and Y. S. Kivshar, Phys. Rev. Lett. **96**, 040401 (2006).

[30] B. A. Malomed, *Soliton Management in Periodic Systems* (Springer, New York, 2006).

[31] J. J. García-Ripoll, V. M. Pérez-García, and P. Torres, Phys. Rev. Lett. **83**, 1715 (1999); J. J. G. Ripoll and V. M. Pérez-García, Phys. Rev. A **59**, 2220 (1999); F. Kh. Abdullaev and J. Garnier, *ibid.* **70**, 053604 (2004); F. Kh. Abdullaev, R. M. Galimzyanov, M. Brtka, and R. A. Kraenkel, J. Phys. B **37**, 3535 (2004).

[32] F. Kh. Abdullaev and R. Galimzyanov, J. Phys. B **36**, 1099 (2003); B. Baizakov, G. Filatrella, B. Malomed, and M. Salerno, Phys. Rev. E **71**, 036619 (2005).

[33] F. Kh. Abdullaev, J. G. Caputo, R. A. Kraenkel, and B. A. Malomed, Phys. Rev. A **67**, 013605 (2003); H. Saito and M. Ueda, Phys. Rev. Lett. **90**, 040403 (2003); G. D. Montesinos, V. M. Perez-Garcia, and P. J. Torres, Physica D **191**, 193 (2004); G. D. Montesinos, V. M. Perez-Garcia, and H. Michinel, Phys. Rev. Lett. **92**, 133901 (2004); A. Itin, T. Morishita, and S. Watanabe, Phys. Rev. A **74**, 033613 (2006).

[34] M. Trippenbach, M. Matuszewski, and B. A. Malomed, Europhys. Lett. **70**, 8 (2005); M. Matuszewski, E. Infeld, B. A. Malomed, and M. Trippenbach, Phys. Rev. Lett. **95**, 050403 (2005).

[35] P. G. Kevrekidis, G. Theocharis, D. J. Frantzeskakis, and B. A. Malomed, Phys. Rev. Lett. **90**, 230401 (2003).

[36] D. A. Zezyulin, G. L. Alfimov, V. V. Konotop, and V. M. Pérez-García, Phys. Rev. A **76**, 013621 (2007).

[37] A. Gubeskys, B. A. Malomed, and I. M. Merhasin, Stud. Appl. Math. **115**, 255 (2005).

[38] F. Kh. Abdullaev, E. N. Tsoy, B. A. Malomed, and R. A. Kraenkel, Phys. Rev. A **68**, 053606 (2003).

[39] H. Saito, R. G. Hulet, and M. Ueda, Phys. Rev. A **76**, 053619 (2007); H. Susanto, P. G. Kevrekidis, B. A. Malomed, and F. Kh. Abdullaev, Phys. Lett. A **372**, 1631 (2008).

[40] T. Mayteevarunyoo, B. A. Malomed, and M. Krairiksh, Phys. Rev. A **76**, 053612 (2007).

[41] G. Burlak and B. A. Malomed, Phys. Rev. A **77**, 053606 (2008).

[42] M. Matuszewski, E. Infeld, B. A. Malomed, and M. Trippenbach, Opt. Commun. **259**, 49 (2006).

[43] F. Kh. Abdullaev, B. B. Baizakov, and M. Salerno, Phys. Rev. E **68**, 066605 (2003); M. Matuszewski, M. Trippenbach, B. A. Malomed, E. Infeld, and A. A. Skorupski, *ibid.* **70**, 016603 (2004); M. I. Rodas-Verde, G. D. Montesinos, H. Michinel, and V. M. Perez-Garcia, J. Opt. Soc. Am. B **23**, 56 (2006).

[44] T. Mayteevarunyoo and B. A. Malomed, Phys. Rev. A **74**, 033616 (2006).

[45] J. H. Denschlag, J. E. Simsarian, H. Häffner, C. McKenzie, A. Browaeys, D. Cho, K. Helmerson, S. L. Rolston, and W. D. Phillips, J. Phys. B **35**, 3095 (2002).

[46] G. G. Carlo, G. Benenti, G. Casati, S. Wimberger, O. Morsch, R. Mannella, and E. Arimondo, Phys. Rev. A **74**, 033617 (2006); T. S. Monteiro, A. Rançon, and J. Ruostekoski, Phys. Rev. Lett. **102**, 014102 (2009).

[47] U. Dorner, P. Fedichev, D. Jaksch, M. Lewenstein, and P. Zoller, Phys. Rev. Lett. **91**, 073601 (2003); L. Fallani, L. De Sarlo, J. E. Lye, M. Modugno, R. Saers, C. Fort, and M. Inguscio, *ibid.* **93**, 140406 (2004).

[48] H. Lignier, C. Sias, D. Ciampini, Y. Singh, A. Zenesini, O. Morsch, and E. Arimondo, Phys. Rev. Lett. **99**, 220403 (2007); C. Sias, H. Lignier, Y. P. Singh, A. Zenesini, D. Ciampini, O. Morsch, and E. Arimondo, *ibid.* **100**, 040404 (2008).

[49] A. Eckardt, M. Holthaus, H. Lignier, A. Zenesini, D. Ciampini, O. Morsch, and E. Arimondo, Phys. Rev. A **79**, 013611 (2009).

[50] A. Zenesini, H. Lignier, D. Ciampini, O. Morsch, and E. Arimondo, Phys. Rev. Lett. **102**, 100403 (2009).

[51] F. Dreisow, A. Szameit, M. Heinrich, T. Pertsch, S. Nolte, A. Tünnermann, and S. Longhi, Phys. Rev. Lett. **101**, 143602 (2008).

[52] I. L. Garanovich, A. A. Sukhorukov, and Y. S. Kivshar, Opt. Express **13**, 5704 (2005); C. R. Rosberg, I. L. Garanovich, A. A. Sukhorukov, D. N. Neshev, W. Królikowski, and Y. S. Kivshar, Opt. Lett. **31**, 1498 (2006).

[53] A. Szameit, I. L. Garanovich, M. Heinrich, A. A. Sukhorukov, F. Dreisow, T. Pertsch, S. Nolte, A. Tünnermann, and Y. S. Kivshar, Phys. Rev. Lett. **101**, 203902 (2008).

[54] I. L. Garanovich, A. Szameit, A. A. Sukhorukov, T. Pertsch, W. Królikowski, S. Nolte, D. Neshev, A. Tünnermann, and Y. S. Kivshar, Opt. Express **15**, 9737 (2007); A. Szameit, Y. V. Kartashov, F. Dreisow, M. Heinrich, T. Pertsch, S. Nolte, A. Tünnermann, V. A. Vysloukh, F. Lederer, and L. Torner, Phys. Rev. Lett. **102**, 153901 (2009).

[55] I. L. Garanovich, A. A. Sukhorukov, and Y. S. Kivshar, Opt. Express **15**, 9547 (2007); A. Szameit, I. L. Garanovich, M. Heinrich, A. Minovich, F. Dreisow, A. A. Sukhorukov, T. Pertsch, D. N. Neshev, S. Nolte, W. Królikowski, A. Tünnermann, A. Mitchell, and Y. S. Kivshar, Phys. Rev. A **78**, 031801(R) (2008).

[56] S. Longhi, Opt. Lett. **30**, 2137 (2005); S. Longhi and K. Staliunas, Opt. Commun. **281**, 4343 (2008); I. L. Garanovich, Phys. Lett. A **372**, 3922 (2008); S. Longhi, M. Marangoni, M. Lobino, R. Ramponi, P. Laporta, E. Cianci, and V. Foglietti, Phys. Rev. Lett. **96**, 243901 (2006); A. Szameit, I. L. Garanovich, M. Heinrich, A. A. Sukhorukov, F. Dreisow, T. Pertsch, S. Nolte, A. Tünnermann, and Y. S. Kivshar, Nat. Photonics **5**, 271 (2009).

[57] K. Shandarova, C. E. Rüter, D. Kip, K. G. Makris, D. N. Christodoulides, O. Peleg, and M. Segev, Phys. Rev. Lett. **102**, 123905 (2009).

[58] G. Kakarantzas, A. Ortigosa-Blanch, T. A. Birks, P. S. Russell, L. Far, F. Couny, and B. J. Mangan, Opt. Lett. **28**, 158 (2003).

[59] C. J. Pethik and H. Smith, *Bose-Einstein Condensation in Dilute Gases* (Cambridge University Press, Cambridge, England, 2002).

[60] C. M. de Sterke and J. E. Sipe, in *Progress in Optics*, edited by E. Wolf (North-Holland, Amsterdam, 1994), Vol. 33, p. 203.

[61] J. Cuevas, B. A. Malomed, P. G. Kevrekidis, and D. J. Frantzeskakis, Phys. Rev. A **79**, 053608 (2009).

[62] B. A. Malomed, Z. H. Wang, P. L. Chu, and G. D. Peng, J. Opt. Soc. Am. B **16**, 1197 (1999); G. L. Alfimov, P. G. Kevrekidis, V. V. Konotop, and M. Salerno, Phys. Rev. E **66**, 046608 (2002).

[63] R. Grimshaw, J. He, and B. A. Malomed, Phys. Scr. **53**, 385 (1996).

[64] D. Anderson, M. Lisak, and T. Reichel, J. Opt. Soc. Am. B **5**, 207 (1988); B. A. Malomed, Prog. Opt. **43**, 69 (2002).

[65] D. J. Kaup, J. El-Reedy, and B. A. Malomed, Phys. Rev. E **50**, 1635 (1994); S. Burtsev, D. J. Kaup, and B. A. Malomed, *ibid.* **52**, 4474 (1995).